

Intertwined Space-Time Symmetry, Orbital Magnetism and Dynamical Berry Curvature in a Circularly Shaken Optical Lattice

Hua Chen^{1,*} and W. Vincent Liu^{2,3,4,†}

¹*Department of Physics, Zhejiang Normal University, Jinhua 321004, China*

²*Department of Physics and Astronomy, University of Pittsburgh, Pittsburgh PA 15260, USA*

³*Wilczek Quantum Center, School of Physics and Astronomy and T. D. Lee Institute, Shanghai Jiao Tong University, Shanghai 200240, China*

⁴*Shenzhen Institute for Quantum Science and Engineering and Department of Physics, Southern University of Science and Technology, Shenzhen 518055, China*

(Dated: December 4, 2020)

We study the circular shaking of a two dimensional optical lattice, which is essentially a (2+1) dimensional space-time lattice exhibiting periodicities in both spatial and temporal dimensions. In particular, the near-resonant shaking technique implemented in the recent experiment at Chicago dynamically activates the p band and reconstructs the low-lying s band by transferring a photon of shaking frequency. The intertwined space-time symmetries are further uncovered to elucidate the degeneracy in the spectrum solved by the generalized Bloch-Floquet theorem. Setting the chirality of circular shaking explicitly breaks the time reversal symmetry and lifts the degeneracy of $p_{\pm} = p_x \pm ip_y$ orbitals, leading to the local circulation of orbital magnetism, *i.e.* the imbalanced orbital content in p_{\pm} orbitals. Moreover, the time evolution of Berry curvature and polarization induced by shaking is purely dynamical. Interestingly, the dynamics is found characterized by a universal phase shift, governed by the time screw rotational symmetry involving a fractional translation of time. These findings suggest that the present lattice shaking scheme provides a versatile platform for the investigation of the orbital physics and the dynamical Berry curvature.

I. INTRODUCTION

Floquet driving provides a promising recipe to realize a periodic structure in the extra dimension of time, generalizing the conventional concept of lattice that is spatially periodic. The Floquet shaken optical lattice [1], which is essentially a space-time lattice with periodic structures in both spatial and temporal dimensions, has been the recent focus of theoretical [2, 3] and experimental [4–6] research for the purpose of synthetic gauge fields [7]. Of particular interest is the lattice-shaking scheme with the near-resonant shaking technique by dynamically activating the p band, which is originally separated from the low-lying s band in the static lattice [8–13]. The recent experimental advance at Chicago leads to a rich variety of interesting phenomena. For instance, a double-well dispersion from the reconstructed band structure through the shaking of one-dimensional optical lattice promotes the quantum simulation of ferromagnetism [9], roton-maxon excitations of Bose-Einstein condensates [10], and the quantum critical dynamics [11, 12]. Later, the shaking scheme is extended to a two-dimensional optical lattice, generalizing the previous experiments in one dimension [13]. Theoretically, the quantum phase transitions in one dimensional shaken lattices is predicted to exhibit a \mathbb{Z}_2 superfluid phase owing to the double-well structure [14]. While, the generalization to two dimensional shaken lattice is nontrivial. The p orbital angular momentum (OAM), which is demonstrated to be the key

attribute of emerging exotic quantum states [15, 16], is quenched in one dimension but is revival in two dimension. The theoretical understanding of the two dimensional shaken lattice remains unexplored and is still currently lacking.

Here we study the (2+1) dimensional space-time lattice that is synthesized by circularly shaking a two dimensional optical lattice with the quasifrequency spectrum being solved by the generalized Bloch-Floquet theorem. Besides the primitive space and time translational symmetries, the intertwined space-time symmetry, which can not be decomposed as a direct product of spatial and temporal symmetries, is uncovered to further reveal the symmetry-protected degeneracy in the quasifrequency spectrum. We also show that the time reversal symmetry breaking, caused by the chirality of circular shaking, lifts the degeneracy between the dynamical activated $p_{\pm} = p_x \pm ip_y$ orbitals, resulting in the local circulation of OAM. Moreover, the time evolution of Berry curvature and polarization induced by the lattice shaking is numerically evaluated. Our results show that the Berry curvature is purely dynamical, signifying the difference from the statical gauge field in the conventional Floquet driving scheme. Last but not least, the frequency-domain analysis reveals that the dynamics is characterized by a universal phase shift, originating from the intertwined space-time symmetry.

The rest of paper is organized as follows. In Sec. II, we solve the Bloch-Floquet spectrum of the (2+1) dimensional space-time lattice. The intertwined space-time symmetry is discussed in Sec. III by revealing the symmetry-protected degeneracy in the Bloch-Floquet spectrum. We also discuss the orbital magnetism and the

* Electronic address: hwachanphy@zjnu.edu.cn

† Electronic address: wvliu@pitt.edu

dynamical Berry curvature in Sec. IV and Sec. V, respectively. Finally, we summarize our results and discuss the possible generalization in Sec. VI.

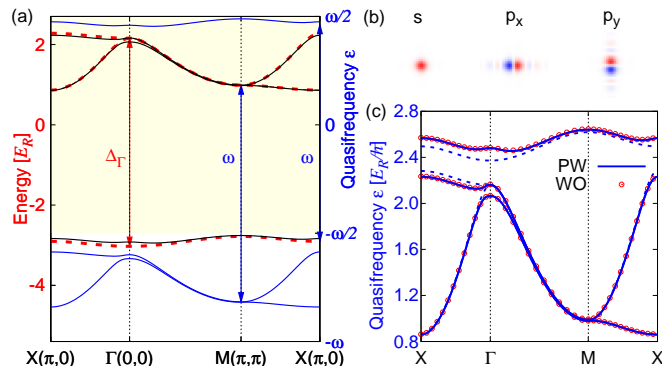


FIG. 1. (a) Band structure along high symmetry lines in the first Brillouin zone. Red dash lines denote to the lowest three Bloch bands of the static potential $\mathcal{V}_0(\mathbf{r})$ in Eq. (5). Solid lines are the Bloch-Floquet bands of the shaking optical potential in Eq. (1). Black and blue lines trace the original and shifted Bloch-Floquet bands due to the shaking, respectively. The first Floquet Brillouin zone $-\omega/2 < \hbar\epsilon \leq \omega/2$ is indicated by yellow shaded region. (b) Spatial distribution of Wannier-orbital wave function for the lowest three Bloch bands. The sign $+(-)$ of wave functions is indicated by red (blue) color. (c) Band structures from plane-wave expansion (blue solid lines) and Wannier-orbital interpolation (open red circles). Blue dash lines are shifted Bloch bands from plane-wave expansion for comparison. The parameters are $\{V, \omega, \theta_s\} = \{4E_R, 5.4E_R, 0.1\}$, where the recoil energy is defined as $E_R = \hbar^2 k_L^2 / 2m$. The higher orbital bands are not shown since their coupling to s orbital band is negligible for the weak shaking.

II. BLOCH-FLOQUET SPECTRUM

We start with the following (2+1)-dimensional optical potential

$$\mathcal{V}(\mathbf{r}, t) = -V \{ \cos[qx - \theta_x(t)] + \cos[qy - \theta_y(t)] \},$$

$$\{ \theta_x(t), \theta_y(t) \} = \theta_s \{ \cos[\omega t], \sin[\omega t] \}, \quad q = 2k_L \quad (1)$$

with k_L being the wave vector of laser beams. It describes that a two-dimensional square optical lattice with lattice depth V and lattice spacing $d = \pi/k_L$ is circularly shaken with shaking amplitudes θ_s and shaking frequencies ω [13]. Without loss of generality, we focus on the shaking with right circular polarization $\boldsymbol{\theta} = (\theta_x, \theta_y)$ in the (2+1) dimensional space-time coordinate. Different chiralities of shaking polarizations are simply connected by a space mirror operation. The optical potential $\mathcal{V}(\mathbf{r}, t)$ in Eq. (1) is invariant under discrete translations with integer multiples of space and time primitive vectors $\{d\hat{x}, d\hat{y}, T\hat{t}\}$ where $T = 2\pi/\omega$ is temporal periodicity. The time-dependent Schrödinger equation $i\hbar\partial_t\psi(\mathbf{r}, t) = \hat{H}(\mathbf{r}, t)\psi(\mathbf{r}, t)$ with $\hat{H}(\mathbf{r}, t) = \hat{\mathbf{p}}^2/2m + \mathcal{V}(\mathbf{r}, t)$ can be

solved by the generalized Bloch-Floquet theorem with its μ -th eigenstate $\psi_{\mu\mathbf{k}}(\mathbf{r}, t) = \exp[i(\mathbf{k} \cdot \mathbf{r} - \epsilon_{\mu\mathbf{k}}t)] u_{\mu\mathbf{k}}(\mathbf{r}, t)$ labelled by quasimomentum \mathbf{k} and quasifrequency $\epsilon_{\mu\mathbf{k}}$. The Bloch-Floquet orbital inherits the periodicities of space-time optical potential $\mathcal{V}(\mathbf{r}, t)$ and takes the form

$$u_{\mu\mathbf{k}}(\mathbf{r}, t) = \sum_{\mathbf{G}\Omega} \exp[i(\mathbf{G} \cdot \mathbf{r} - \Omega t)] u_{\mu\mathbf{k}}^{\mathbf{G}\Omega} \quad (2)$$

with \mathbf{G} and Ω being the reciprocal space and time vectors, respectively. Following the Floquet theory, the time-dependent Schrödinger equation is then converted into an eigenvalue problem

$$\sum_{\mathbf{G}'\Omega'} \hat{K}_{\mathbf{G}\Omega, \mathbf{G}'\Omega'} u_{\mu\mathbf{k}}^{\mathbf{G}'\Omega'} = \hbar\epsilon_{\mu\mathbf{k}} u_{\mu\mathbf{k}}^{\mathbf{G}\Omega} \quad (3)$$

with

$$\hat{K}_{\mathbf{G}\Omega, \mathbf{G}'\Omega'} = \left[\frac{(\hbar\mathbf{k} + \hbar\mathbf{G})^2}{2m} - \hbar\Omega \right] \delta_{\mathbf{G}\Omega, \mathbf{G}'\Omega'} + \mathcal{V}_{\mathbf{G}-\mathbf{G}'\Omega-\Omega'}$$

$$(4)$$

being the Floquet operator $\hat{K}(\mathbf{r}, t) = \hat{H}(\mathbf{r}, t) - i\hbar\partial_t$ in the Fourier-transformed bases [17, 18]. Here $\mathcal{V}_{\mathbf{G}\Omega}$ are the Fourier component of the space-time potential $\mathcal{V}(\mathbf{r}, t)$. Before proceeding, it is instructive to discuss the optical potential in temporal series $\mathcal{V}(\mathbf{r}, t) = \sum_n \mathcal{V}_n(\mathbf{r}) \exp[-in\omega t]$ with

$$\mathcal{V}_n(\mathbf{r}) = -V_n \times \begin{cases} -i^{n+1} \sin(qx) + i \sin(qy) & n \text{ odd} \\ i^n \cos(qx) + \cos(qy) & n \text{ even} \end{cases} \quad (5)$$

where $V_n = V J_n(\theta_s)$ is the effective potential and $J_n(x)$ is the Bessel function of first kind. The zeroth-order optical potential $\mathcal{V}_{n=0}(\mathbf{r})$ gives rise to a static square optical potential with effective potential $V_0 = V J_0(\theta_s)$. The corresponding Bloch band structure is shown in Fig. 1(a). For the lowest three bands, Wannier orbitals are further constructed to reveal the band characters

$$u_{\mu\mathbf{R}}(\mathbf{r}) = \sum_{\mathbf{k}} \exp[i\mathbf{k} \cdot \mathbf{R}] \bar{\psi}_{\mu\mathbf{k}}(\mathbf{r}), \quad (6)$$

where \mathbf{R} specifies the center of Wannier orbitals and $\bar{\psi}_{\mu\mathbf{k}}(\mathbf{r})$ is the μ -th Bloch band state of the static potential $\mathcal{V}_{n=0}(\mathbf{r})$ in Eq. (5) in the Wannier gauge. Technique details are presented in Appendix A. The lowest and upper two bands are characterized by s and (p_x, p_y) orbitals, respectively. Their spatial distributions of wave functions are depicted in Fig. 1(b). Upon shaking, the Bloch bands are repeatedly shifted by shaking frequency ω and are hybridized by the dynamical optical potential $\mathcal{V}_{n \neq 0}(\mathbf{r})$. As sketched in Fig. 1(a), we focus on the blue detuned case $\omega \gtrsim \Delta_\Gamma$ that the shaking frequency ω is slightly higher than the direct band gap Δ_Γ between s and (p_x, p_y) bands at Γ point, which is realized in the experiment at Chicago [13]. In the weak shaking limit $\theta_s \ll 1$, the effective potential of high order V_n is severely suppressed by the asymptotic behavior of Bessel function $J_{|n|}(x) \approx (x/2)^{|n|} / \Gamma(|n| + 1)$, where $\Gamma(x)$ is the

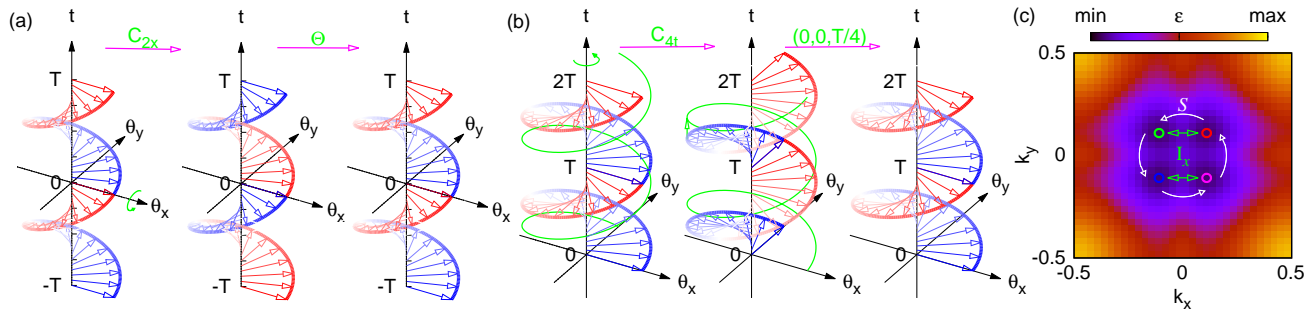


FIG. 2. Trajectory of shaking phase $\boldsymbol{\theta}(t) = (\theta_x(t), \theta_y(t))$ in Eq. (1) to illustrate (a) intertwined space-time operation $\mathcal{I}_x = \Theta\{C_{2x}|\mathbf{0}\}$ composed of a space-time rotation of π about x axis followed by a time reversal Θ , and (b) time screw rotation $\mathcal{S} = \{C_{4t}|\mathbf{0}, 0, T/4\}$ composed of a spatial rotation of $\pi/2$ about the temporal axis t followed by a time translation $T/4$. (c) Landscape of the quasifrequency ϵ for the s Bloch-Floquet band with four degenerate band minima (valleys) being indicated by open circles. The parameters are chosen as $\{V, \omega, \theta_s\} = \{4E_R, 5.4E_R, 0.1\}$. Illustration of the symmetry-protected degenerated states at different quasimomenta.

gamma function. In practice, the optical potential $\mathcal{V}_n(\mathbf{r})$ in our numerical simulations are truncated up to $|n| = 1$. As shown in Fig. 1(c), the s and (p_x, p_y) bands are hybridized by the dynamical optical potential $\mathcal{V}_{n=\pm 1}(\mathbf{r})$ according to the selection rule described in Ref. [19]. The Bloch-Floquet band structure calculated by plane-wave expansion and Wannier-orbital interpolation shows excellent agreement with each other.

III. INTERTWINED SPACE-TIME SYMMETRY

Having established the Bloch-Floquet band structure, we next show that the present (2+1)-dimensional system possesses a D_4 space-time symmetry. Besides the primitive spatial and temporal translational symmetry discussed above, the intertwined space-time symmetries are essential to understand the degeneracy of the quasifrequency spectrum at different quasimomenta connected the symmetry operation. To facilitate our discussion, we adopt a (2+1)-dimensional space-time vector (\mathbf{r}, t) to define a space-time operation

$$\{g|\boldsymbol{\tau}\}(\mathbf{r}, t) = g(\mathbf{r}, t) + \boldsymbol{\tau}, \quad (7)$$

where g and $\boldsymbol{\tau}$ denote point group operations and translational vectors, respectively. The D_4 space-time group has two group generators in total. As depicted in Fig. 2(a), the first generator is

$$\mathcal{I}_x = \Theta\{C_{2x}|\mathbf{0}\}, \quad (8)$$

which is a space-time rotation of π about x axis that sends the space-time vector (\mathbf{r}, t) to $(x, -y, -t)$, followed by time reversal Θ . For spinless bosons involved in the experiment at Chicago [13], the time reversal operator is mathematically described by complex conjugate $\Theta = \mathcal{K}$. It is worth remarking that the symmetry discussed here refers to the space-time transformation $\hat{U}(\mathbf{r}, t)$ under

which the Floquet operator $\hat{K} = \hat{\mathcal{H}} - i\hbar\partial_t$ is left invariant. As depicted in Fig. 2(b), the second generator of D_4 space-time group is the time screw rotation

$$\mathcal{S} = \{C_{4t}|\mathbf{0}, 0, T/4\}. \quad (9)$$

It describes a spatial rotation of $\pi/2$ about the temporal axis t , which sends the space-time vector (\mathbf{r}, t) to $(-y, x, t)$, followed by a fractional primitive translation of time $T/4$. These two symmetries have crucial implications on the Bloch-Floquet band structure. To illustrate, we focus on the s Bloch-Floquet band that is adiabatically connected to the s band in the non-shaking limit. The symmetry prediction is however not limited to this band. As shown in Fig. 2(c), the intertwined space-time symmetry \mathcal{I}_x ensures an identical spectrum at quasimomenta (k_x, k_y) and $(-k_x, k_y)$ by constructing an explicit connection between their Bloch-Floquet orbital wave functions. Similarly, the time screw rotational symmetry \mathcal{S} connects the states at (k_x, k_y) and $(-k_y, k_x)$. Detailed proofs are provided in Appendix B. Particular attention should be paid to four degenerated band minima (dubbed valleys), which are fully connected by the space-time symmetries. These valleys arise from the dynamical hybridization of s and (p_x, p_y) orbitals due to the lattice shaking, and are generally incommensurate to the optical lattice. The single-particle ground state, constructed by the linear superposition of the wave functions at these valleys, is on an infinitely degenerate manifold. This single-particle degeneracy can be lifted by many-body interactions through spontaneous symmetry breaking. Experimentally, bosons are found to be condensed into the valley polarized state, and segregate into domains with each condensing into one of the valleys [13]. This is different from the commensurate case that the intervalley exchange interaction promoted by the Umklapp scattering process supports the valley coherent Bose-Einstein condensation [20].

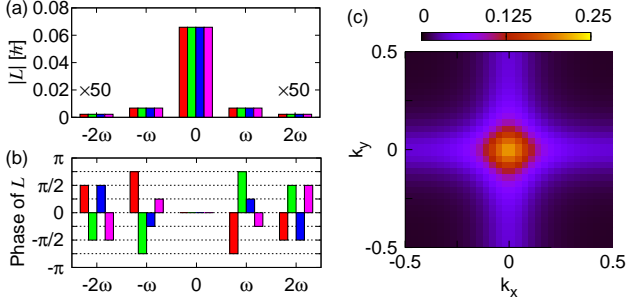


FIG. 3. (a) Amplitude and (b) phase of the complex-valued local circulation of orbital angular momentum $L(\mathbf{k}, \Omega)$ in Eq. (11) at four valleys with the bar colors indicated in Fig. 2(c). (c) Static orbital angular momentum $L(\mathbf{k}, \Omega = 0)$ in the first Brillouin zone for s Bloch-Floquet band. The parameters in numerical calculations are $\{V, \omega, \theta_s\} = \{4E_R, 5.4E_R, 0.1\}$.

IV. ORBITAL MAGNETISM

The chirality of shaking polarization in Eq. (1) explicitly breaks the time-reversal symmetry, which leads to the generation of orbital magnetism, *i.e.* the imbalanced orbital content in $p_{\pm} = p_x \pm ip_y$ orbitals. To gain an intuitive understanding, we take a close inspection on the optical potential in temporal series. In polar coordinates (r, θ) , the leading order

$$\mathcal{V}_{n=\pm 1}(\mathbf{r}) = \mp V_{\pm 1} \sum_{\ell \text{ odd}} (i^{\ell-1} \pm 1) J_{\ell}(qr) \exp[i\ell\theta] \quad (10)$$

locally couples the s and $p_{+} = p_x + ip_y$ orbitals by the selection rule of OAM [21]. It is worth remarking that the coupling between s and $p_{-} = p_x - ip_y$ orbitals is prohibited by the temporal selection rule [19] and originates from the time-reversal symmetry breaking. Consequently, the degeneracy lifting between the p_{\pm} Wannier orbitals leads the local circulation of OAM around the static lattice sites in the bulk, which is extensively studied in electronic solids in the context of orbital magnetism [22–27]. Here we extend the microscopic derivation on the local circulation of OAM by explicitly calculating the contribution of a single Bloch-Floquet state, which is crucial for the valley polarized Bose-Einstein condensation. More interestingly, the OAM studied here is inherently dynamical due to the lattice shaking, which sets our study apart from the previous studies on static lattices. The contribution of s Bloch-Floquet state $\psi_{s\mathbf{k}}(\mathbf{r}, t)$ in frequency domain is mathematically described by

$$L(\mathbf{k}, \Omega) = \frac{1}{\mathcal{N}_{\text{uc}}} \sum_{\mathbf{R}} \frac{1}{T} \int_0^T dt \langle \psi_{s\mathbf{k}} | \hat{L}_{\mathbf{R}}^z | \psi_{s\mathbf{k}} \rangle \exp[i\Omega t], \quad (11)$$

where $\hat{L}_{\mathbf{R}} = (\mathbf{r} - \mathbf{R}) \times \hat{\mathbf{p}}$ is the OAM operator around the static lattice sites \mathbf{R} and \mathcal{N}_{uc} is the number of unit

cells. A lengthy but straightforward algebra leads to the explicit expression

$$L(\mathbf{k}, \Omega' - \Omega) = -i\hbar \sum_{\mathbf{G} \neq \mathbf{G}'} \sum_{\Omega''} u_{s\mathbf{k}}^{\mathbf{G}\Omega''*} u_{s\mathbf{k}}^{\mathbf{G}'\Omega''} \times \left\{ \exp\left[-i(G'_x - G_x) \frac{d}{2}\right] \frac{k_y + G'_y}{G'_x - G_x} \delta_{G_y, G'_y} - x \leftrightarrow y \right\}.$$

Figures 3(a) and 3(b) show the numerical evaluation of $L(\mathbf{k}, \Omega)$ at four valleys. The static OAM dominates while the high frequency component at $\Omega = \pm 2\omega$ is vanishingly small. The phase of dynamical OAM at neighbouring valleys differs by $\pi/2$ and π for $\Omega = \pm\omega$ and $\pm 2\omega$, respectively. This phase shift between valleys is dictated by the fractional translation of time $T/4$ in the time screw rotation symmetry \mathcal{S} and thus serves as a signature of the intertwined space-time symmetry. The static OAM in the first Brillouin zone shown Fig. 3(c) reaches its maximum at Γ point where the coupling between s and p_{+} orbitals is most significant.

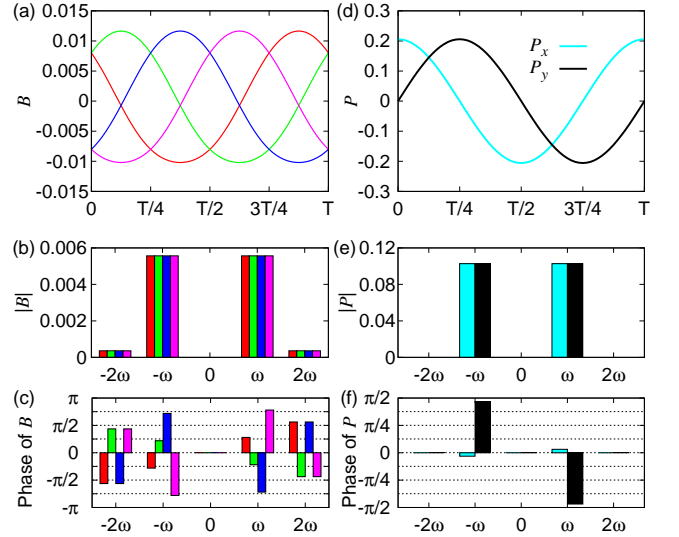


FIG. 4. (a) Time evolution of Berry curvature $\mathcal{B}(\mathbf{k}, t)$ in Eq. (12), (b) amplitude and (c) phase of the complex-valued Berry curvature $\mathcal{B}(\mathbf{k}, \Omega)$ in Eq. (13) at four valleys with the colors indicated in Fig. 2(c). (d) Time evolution of dynamical polarization $\mathcal{P}(t)$ in Eq. (14), (e) amplitude and (f) phase of the complex-valued polarization $\mathcal{P}(\Omega)$ in Eq. (15) for s Bloch-Floquet band. The parameters are taken as $\{V, \omega, \theta_s\} = \{4E_R, 5.4E_R, 0.1\}$.

V. DYNAMICAL BERRY CURVATURE

Besides the local circulation of OAM, the circular shaking also introduces a dynamical Berry curvature (BC) in s Bloch-Floquet band

$$\mathcal{B}(\mathbf{k}, t) = \nabla_{\mathbf{k}} \times \mathcal{A}_{\mathbf{k}}(t), \quad (12)$$

where $\mathcal{A}_{\mathbf{k}}(t) = i \langle u_{s\mathbf{k}}(\mathbf{r}, t) | \nabla_{\mathbf{k}} | u_{s\mathbf{k}}(\mathbf{r}, t) \rangle$ is the dynamical Berry connection. The BC is numerically evaluated based on an efficient method in discretized Brillouin zone [28]. As depicted in Fig. 4(a), the time evolution of BC $\mathcal{B}(\mathbf{k}, t)$ at four valleys shows an oscillating behaviour. For the valley polarized Bose-Einstein condensation, the dynamical BC can be in principal detected by measuring the transverse shift of anomalous velocity $\mathcal{F} \times \mathcal{B}(\mathbf{k}, t)$ with an external force \mathcal{F} , which can be engineered by a slowly varying optical potential [29, 30]. This transverse shift resembles that of charged particles under ac magnetic fields. The dynamics is quantitatively characterized by introducing the Fourier-transformed BC

$$\mathcal{B}(\mathbf{k}, \Omega) = \frac{1}{T} \int_0^T dt \mathcal{B}(\mathbf{k}, t) \exp[i\Omega t] \quad (13)$$

in the frequency domain. As shown in Fig. 4(b), the dynamical BC is dominated at the frequency $\Omega = \pm\omega$ with a vanished static component, which is in stark contrast with the dynamics of the local circulation of OAM. The phase shift of BC between neighbouring valleys in Fig. 4(c) follows the prediction of intertwined space-time symmetry that we discussed above. Interestingly, the predicted phase shift here can be simultaneously determined for segregated domains with each condensing into one of four valleys in the experiments [13]. Alternatively, the dynamical BC induced by the circular shaking can be also detected by measuring the dynamical polarization [31, 32]

$$\mathcal{P}(t) = \frac{1}{2\pi} \int_{\text{BZ}} d\mathbf{k} \mathcal{A}_{\mathbf{k}}(t), \quad (14)$$

which is also proportional to the center of mass of the instantaneous Wannier functions [33]. Figure 4(d) shows the numerical results on the time evolution of dynamical polarization, which is locked in phase with the circular driving. Similarly, the frequency-domain analysis applies to the dynamical polarization

$$\mathcal{P}(\Omega) = \frac{1}{T} \int_0^T dt \mathcal{P}(t) \exp[i\Omega t]. \quad (15)$$

Figures 4(e) and 4(f) show that the dynamical polarization oscillates at frequency $\Omega = \pm\omega$ with an universal $\pi/2$ phase shift between $\mathcal{P}_x(\pm\omega)$ and $\mathcal{P}_y(\pm\omega)$. Experimentally, the dynamical polarization can be determined by measuring the center of mass position of ultracold atoms through the in situ image. For instance, such a measurement was done in the s Bloch-Floquet band that is completely filled with fermionic atoms [34].

VI. SUMMARY AND OUTLOOK

To summarize, we have studied the intertwined space-time symmetries as well as their implication on the dynamics for the recent experimental implement of the circularly shaken optical lattice. In particular, the time

screw rotation symmetry studied here can be easily generalized to n -fold spatial rotational axis in the presence of a circularly polarized ac field. The symmetry-protected phase shift is generally applicable as a universal feature of the dynamical response for these systems. We also propose the experimental detection of orbital angular momentum and dynamical Berry curvature, which was so far not measured quantitatively. Our study mainly focusing on the symmetry aspect serves as a starting point for future studies, *e.g.* out-of-equilibrium with dissipations.

ACKNOWLEDGEMENT

We thank Cheng Chin, Logan W. Clark, and Kai-Xuan Yao for helpful discussions. This work is supported by National Natural Science Foundation of China under Grants No. 11704338 and No. 11835011 (H. C.), and by AFOSR Grant No. FA9550-16-1-0006, MURI-ARO Grant No. W911NF-17-1-0323 through UC Santa Barbara, and Shanghai Municipal Science and Technology Major Project (Grant No. 2019SHZDZX01) (W.V. L.).

Appendix A: Wannier orbital construction

The approach of Wannier orbitals for the solid-state materials has relied on the well established Marzari-Vanderbilt scheme [35–37], and is numerically implemented into a numerical package [38]. The Wannier states are determined by numerically minimizing the spatial spread functional to find the optimal unitary transformation into the Wannier basis. Here, we adopt an alternative numerical method based on Refs. [39, 40] to calculate Wannier states for the static optical $\mathcal{V}_{n=0}(\mathbf{r})$ in Eq. (5), reducing the problem to the diagonalization of a matrix. This intrinsically avoids the possible problem of trapping in local minima during the numerical minimization and is numerically highly efficient.

Following Refs. [39, 40], the Wannier orbitals are the eigenstates of the Resta's position operator $\hat{R} = \exp[-i\Delta\mathbf{k} \cdot \mathbf{r}]$, which satisfies the periodic boundary condition. In the Bloch band basis, the matrix elements of the operator \hat{R} can be expressed as the real-space integrals over the entire spatial region

$$R_{\mathbf{k}\mathbf{k}'}^{\mu\mu'} = \frac{1}{L_x L_y} \int d\mathbf{r} \psi_{\mu\mathbf{k}}^*(\mathbf{r}) \hat{R} \psi_{\mu'\mathbf{k}'}(\mathbf{r}), \quad (A1)$$

where $\psi_{\mu\mathbf{k}}(\mathbf{r})$ are the Bloch states of the static potential. The real-space integration can be calculated analytically. We arrive at

$$R_{\mathbf{k}\mathbf{k}'}^{\mu\mu'} = \sum_{\mathbf{G}\mathbf{G}'} \delta_{\mathbf{k}+\mathbf{G}+\Delta\mathbf{k}, \mathbf{k}'+\mathbf{G}'} u_{\mu\mathbf{k}}^{\mathbf{G}*} u_{\mu'\mathbf{k}'}^{\mathbf{G}'}, \quad (A2)$$

where $u_{\mu\mathbf{k}}^{\mathbf{G}}$ are the Bloch orbitals of the static potential. Moreover, the separability of the static optical potential

$$\mathcal{V}_{n=0}(\mathbf{r}) = -V_0 [\cos(qx) + \cos(qy)] \quad (A3)$$

ensures the commutation relation of the position operators $[\hat{X}, \hat{Y}] = 0$. Therefore, the two-dimensional Wannier orbitals can be obtained simultaneously by successively diagonalizing the corresponding matrices X and Y in Eq. (A2).

Appendix B: Intertwined space-time symmetry

In the following, we provide the detailed proof of the intertwined space-time symmetry for the implication on the Bloch-Floquet spectrum. With the generalized Bloch-Floquet theorem, the time-dependent Schrödinger equation is recast to the following equation

$$\hat{K}(\mathbf{r}, t) \exp[i\mathbf{k} \cdot \mathbf{r}] u_{\mu\mathbf{k}}(\mathbf{r}, t) = \hbar\epsilon_{\mu\mathbf{k}} \exp[i\mathbf{k} \cdot \mathbf{r}] u_{\mu\mathbf{k}}(\mathbf{r}, t) \quad (\text{B1})$$

with the Floquet operator

$$\hat{K}(\mathbf{r}, t) = \hat{\mathcal{H}}(\mathbf{r}, t) - i\hbar\partial_t. \quad (\text{B2})$$

First, we shall focus on the time screw rotation

$$\mathcal{S}(x, y, t) = \left(-y, x, t + \frac{T}{4}\right). \quad (\text{B3})$$

It is easy to check that the Floquet operator is invariant under the time screw rotation $\mathcal{S}^\dagger \hat{\mathcal{K}}(\mathbf{r}, t) \mathcal{S} =$

$\hat{\mathcal{K}}(\mathbf{r}, t)$, which ensures that both $\mathcal{S} \exp[i\mathbf{k} \cdot \mathbf{r}] u_{\mu\mathbf{k}}(\mathbf{r}, t)$ and $\exp[i\mathbf{k} \cdot \mathbf{r}] u_{\mu\mathbf{k}}(\mathbf{r}, t)$ are the eigenstates of Eq. (B1) and share an identical quasifrequency. On the other hand, the simple relation

$$\mathcal{S} \exp[i\mathbf{k} \cdot \mathbf{r}] u_{\mu\mathbf{k}}(\mathbf{r}, t) = \exp[i(-k_y, k_x) \cdot \mathbf{r}] \mathcal{S} u_{\mu\mathbf{k}}(\mathbf{r}, t) \quad (\text{B4})$$

indicates that $\mathcal{S} u_{\mu\mathbf{k}}(\mathbf{r}, t)$ is the eigenstate of Eq. (B1) with quasimomentum $(-k_y, k_x)$. Therefore, the degeneracy between quasimomenta $(-k_y, k_x)$ and \mathbf{k} is established with their eigenstates obeying

$$u_{\mu(-k_y, k_x)}^{(-G_y, G_x)\Omega} \propto u_{\mu\mathbf{k}}^{\mathbf{G}\Omega} \exp\left[\frac{1}{4}i\Omega T\right]. \quad (\text{B5})$$

It is worth remarking that the phase shift discussed in Sec. IV and Sec. V is dictated by the twist phase $\exp[i\Omega T/4]$ in Eq. (B5).

Second, we would like to briefly discuss the intertwined space-time symmetry

$$\mathcal{I}_x = \Theta\{C_{2x}|\mathbf{0}\}. \quad (\text{B6})$$

Similar analysis shows that the states $\mathcal{I}_x u_{\mu\mathbf{k}}(\mathbf{r}, t)$ and $u_{\mu\mathbf{k}}(\mathbf{r}, t)$ share an identical quasifrequency with the following relation on their Fourier components

$$u_{\mu(-k_x, k_y)}^{(-G_y, G_x)\Omega} \propto u_{\mu\mathbf{k}}^{\mathbf{G}\Omega*} \quad (\text{B7})$$

between quasimomenta $(-k_x, k_y)$ and \mathbf{k} .

-
- [1] A. Eckardt, *Rev. Mod. Phys.* **89**, 011004 (2017).
[2] J. Dalibard, F. Gerbier, G. Juzeliūnas, and P. Öhberg, *Rev. Mod. Phys.* **83**, 1523 (2011).
[3] N. Goldman, J. C. Budich, and P. Zoller, *Nature Physics* **12**, 639 (2016).
[4] G. Jotzu, M. Messer, R. Desbuquois, M. Lebrat, T. Uehlinger, D. Greif, and T. Esslinger, *Nature* **515**, 237 (2014).
[5] N. Fläschner, B. S. Rem, M. Tarnowski, D. Vogel, D.-S. Lühmann, K. Sengstock, and C. Weitenberg, *Science* **352**, 1091 (2016).
[6] K. Wintersperger, C. Braun, F. N. Ünal, A. Eckardt, M. D. Liberto, N. Goldman, I. Bloch, and M. Aidelsburger, *Nature Physics* **10.1038/s41567-020-0949-y** (2020).
[7] N. R. Cooper, J. Dalibard, and I. B. Spielman, *Rev. Mod. Phys.* **91**, 015005 (2019).
[8] N. Gemelke, E. Sarajlic, Y. Bidet, S. Hong, and S. Chu, *Phys. Rev. Lett.* **95**, 170404 (2005).
[9] C. V. Parker, L.-C. Ha, and C. Chin, *Nature Physics* **9**, 769 (2013).
[10] L.-C. Ha, L. W. Clark, C. V. Parker, B. M. Anderson, and C. Chin, *Phys. Rev. Lett.* **114**, 055301 (2015).
[11] L. W. Clark, L. Feng, and C. Chin, *Science* **354**, 606 (2016).
[12] L. Feng, L. W. Clark, A. Gaj, and C. Chin, *Nature Physics* **14**, 269 (2018).
[13] L. W. Clark, B. M. Anderson, L. Feng, A. Gaj, K. Levin, and C. Chin, *Phys. Rev. Lett.* **121**, 030402 (2018).
[14] W. Zheng, B. Liu, J. Miao, C. Chin, and H. Zhai, *Phys. Rev. Lett.* **113**, 155303 (2014).
[15] M. Lewenstein and W. V. Liu, *Nature Physics* **7**, 101 (2011).
[16] X. Li and W. V. Liu, *Reports on Progress in Physics* **79**, 116401 (2016).
[17] J. H. Shirley, *Phys. Rev.* **138**, B979 (1965).
[18] H. Sambe, *Phys. Rev. A* **7**, 2203 (1973).
[19] M. S. Rudner, N. H. Lindner, E. Berg, and M. Levin, *Phys. Rev. X* **3**, 031005 (2013).
[20] H. Chen, *Phys. Rev. A* **101**, 063601 (2020).
[21] H. Chen and X. C. Xie, *Phys. Rev. A* **98**, 053611 (2018).
[22] D. Xiao, J. Shi, and Q. Niu, *Phys. Rev. Lett.* **95**, 137204 (2005).
[23] T. Thonhauser, D. Ceresoli, D. Vanderbilt, and R. Resta, *Phys. Rev. Lett.* **95**, 137205 (2005).
[24] D. Ceresoli, T. Thonhauser, D. Vanderbilt, and R. Resta, *Phys. Rev. B* **74**, 024408 (2006).
[25] J. Shi, G. Vignale, D. Xiao, and Q. Niu, *Phys. Rev. Lett.* **99**, 197202 (2007).
[26] D. Xiao, M.-C. Chang, and Q. Niu, *Rev. Mod. Phys.* **82**, 1959 (2010).
[27] T. Thonhauser, *Int. J. Mod. Phys. B* **25**, 1429 (2011).
[28] T. Fukui, Y. Hatsugai, and H. Suzuki, *Journal of the Physical Society of Japan* **74**, 1674 (2005).

- [29] A. Dauphin and N. Goldman, *Phys. Rev. Lett.* **111**, 135302 (2013).
- [30] M. Aidelsburger, M. Lohse, C. Schweizer, M. Atala, J. T. Barreiro, S. Nascimbène, N. R. Cooper, I. Bloch, and N. Goldman, *Nature Physics* **11**, 162 (2015).
- [31] R. Resta and D. Vanderbilt, Theory of polarization: A modern approach, in *Physics of Ferroelectrics: A Modern Perspective* (Springer Berlin Heidelberg, Berlin, Heidelberg, 2007).
- [32] D. Vanderbilt, *Berry Phases in Electronic Structure Theory: Electric Polarization, Orbital Magnetization and Topological Insulators* (Cambridge University Press, 2018).
- [33] B. Huang and W. V. Liu, *Phys. Rev. Lett.* **124**, 216601 (2020).
- [34] M. Lohse, C. Schweizer, O. Zilberberg, M. Aidelsburger, and I. Bloch, *Nature Physics* **12**, 350 (2016).
- [35] N. Marzari and D. Vanderbilt, *Phys. Rev. B* **56**, 12847 (1997).
- [36] I. Souza, N. Marzari, and D. Vanderbilt, *Phys. Rev. B* **65**, 035109 (2001).
- [37] N. Marzari, A. A. Mostofi, J. R. Yates, I. Souza, and D. Vanderbilt, *Rev. Mod. Phys.* **84**, 1419 (2012).
- [38] A. A. Mostofi, J. R. Yates, Y.-S. Lee, I. Souza, D. Vanderbilt, and N. Marzari, *Computer Physics Communications* **178**, 685 (2008).
- [39] S. Kivelson, *Phys. Rev. B* **26**, 4269 (1982).
- [40] R. Resta, *Phys. Rev. Lett.* **80**, 1800 (1998).